Cano-Pleite, E., et al. Reversal of gulf stream circulation in a vertically vibrated triangular fluidized bed, In: *Powder Technology, Vol. 316, July 2017, Pp. 345-356 (special issue Fluidization XV Conference, Montebello, Canada, May 22th to 27th, 2016: Proceedings)*
DOI: https://doi.org/10.1016/j.powtec.2017.01.007

Reversal of gulf stream circulation in a vertically vibrated triangular fluidized bed

E. Cano-Pleite[a,*], F. Hernández-Jiménez[a], A. Acosta-Iborra[a], C.R. Müller[b]

[a] *Carlos III University of Madrid, Department of Thermal and Fluids Engineering. Av. de la Universidad 30, 28911, Leganés, Madrid, Spain*
[b] *ETH Zurich, Institute of Energy Technology, Laboratory of Energy Science and Engineering, Leonhardstrasse 21, 8092 Zurich, Switzerland*

Abstract

The present work experimentally assesses the effect of vibration on the dynamics of particles in a fluidized bed of triangular shape. The base of the bed is composed of two inclined walls, each one forming an angle of 45° with the horizontal. The bed has 0.206 m span and 0.01 m thickness. The bed vessel is made of antistatic PMMA in order to allow optical access with a high-speed camera. The bed is mounted on an electrodynamic shaker which produces vertical vibration. The bed material is ballotini particles with a mean diameter of 1.15 mm up to the top of the inclined walls. Air was injected through the inclined bed walls to fluidize the bed to explore whether vibration of the bed vessel together with gas injection can make the dynamics of this bed different to that found when no gas is injected. A high speed camera was used to record the motion of particles in the bed. The velocity of the particles in the bed was obtained via Particle Image Velocimetry (PIV). The results show that several circulation patterns are observed as a function of vibration amplitude and frequency when the fluidization velocity is just below and above the minimum fluidization velocity. Noticeably, for zero gas velocity, particles ascend close to the side walls and descend in the center of the bed. By injecting fluidization gas, the circulation pattern of the bed can be reversed (i.e. particles descending near the inclined walls and ascending in the center of the bed). Conditions for which this reversal of the gulf stream circulation of particles appear in the triangular bed are explored in this work and these include gas superficial velocities higher than the minimum fluidization velocity and sufficiently high values of the vibration strength.

Keywords: Fluidization, Vibration, Triangular bed, Gulf stream circulation

1. Introduction

The introduction of vibration to granular systems can intensify certain processes [1, 2] and increase the efficiency of chemical reactors [3–7]. However, when vibration energy is introduced in a granular assembly,

*Corresponding author. Tel:+34 91 624 8884
Email address: edcanop@ing.uc3m.es (E. Cano-Pleite)

a great variety of phenomena can appear [8]. These phenomena include heaping or tilting of the granular surface of the bed to the center or to one of the laterals of the bed [9–12, 14], the formation of convection rolls of particles in the bed, whose number and direction depend on the vibration characteristics [10, 14–19] and subharmonic instabilities. Examples of these instabilities are waves on the surface of the bed, which may manifest at different frequencies [11, 12, 20, 21] and cyclic detaching of the solids bulk from the bed vessel forming arching structures [22–25]. Among the different phenomena associated to vibration of the granular bed, convection of particles is one of the most important and has been profusely studied both experimentally and numerically [10, 14–19].

Akiyama et al. [19] presented an experimental study on the role of the interstitial gas on the convective motion and heaping in a vibrated granular bed of 100 x 200 x 30 mm^3 filled with glass beads of eight different diameters. In their experiments, they observed a convective roll (i.e. recirculation of particles) extended through the whole bed. Their results show that the amount of gas trapped in the bed, and, thus, the mobility of the particles, play a key role on the developing of the convective flow in the bed. Aoki et al. [17, 18], observed the formation of multiple convective rolls in a bed of similar dimensions to the one in [19]. They showed that the formation of arching structures in the bed is crucial for the appearance of convection rolls in the bed. Interestingly, they found that when Γ exceeded a critical value, the convection mode near to the vertical side walls changed form downward to upward convection. Zhang et al. [10] experimentally studied the patterns of convective flow formed in a vibrated granular bed of 300 x 200 x 20 mm^3 filled with particles of 1, 2 and 4.5 mm of diameter. They observed that, when varying the frequency of vibration, within the range 15 to 150 Hz, a wide range of convective patterns appeared in the granular layer. A phase map of Γ versus frequency, f, was drawn in [10] in order to understand the different patterns observed.

The appearance of granular patterns in vibrated beds is not only restricted to square-shaped beds. Recently, Lu et al. [26], studied the formation of polygon shaped patterns in a pseudo-2D (i.e. bed of small thickness) vibrated bed of circular section with particles of 0.3-0.4 mm and 0.5-0.75 mm of diameter and different fill levels. In their work, they identified a variety of granular patterns such as Faraday tilting, surface waves having 1/2 and 1/4 the frequency of vibration of the bed vessel, convection and polygonal structures. They proposed that the polygon-shaped patterns are the geometrical transformation of the arching structures typically encountered in vibrated beds of rectangular vertical section. Knight et al. [27], studied the vibration-induced size separation in a vibrated granular media in both a rectangular and a conical bed filled with spherical particles of 2 mm of diameter. They observed that convection drives size segregation and, to confirm their hypothesis, they designed a conical container. In that container they observed that vibration promoted a convective motion of particles upwards along the walls and downwards in the middle of the container. The same convective pattern of particles was observed by Wassgren et al. [28] in a vibrated pseudo-2D hopper of wedge shape (triangular) with the exit closed and filled with soda lime particles of 1.3 mm of mean diameter. Discrete elements simulations of the hopper revealed that the

convective motion is caused by the dilation of the particle bed during free fall period of the vibration cycle and the interaction with the hopper walls [28]. They also detected the formation of $f/2$ waves in the surface of the vibrated hopper, similar to those observed in vibrated rectangular beds.

Although these convection patterns have been studied in conical hoppers, the effect of injecting gas through the inclined lateral walls on the overall convection patterns is currently unexplored. It is conceivable that the injection of gas may alter the convection pattern and hence, in turn, also the characteristics times in such systems. The potential use of this triangular geometry with background gas injection can be similar to that of either aerated hoppers [29–34] or spout-fluidized beds with inclined walls, namely cylindrical spout-fluidized beds [35–38]. The injection of gas through the inclined walls of this kind of beds, even if the bed walls are not vibrated, has demonstrated to improve their performance.

Aerated hoppers are often used to avoid undesirable phenomena such as arching and funnel-flow in hoppers operating with fine particles. In these hoppers, the discharge rate can be increased when aerating the bed until a gas flow was reached, after which the discharge rate becomes constant [32, 33]. It was also detected that different regimes may appear in the hopper depending on the aeration rate [29–31].

In spout-fluidized beds, in addition of the spouting gas, background gas is injected through the base or the inclined walls of the bed. Thus, this type of beds combines the favorable properties of both spouted and fluidized beds and have received great interest in the last decades in applications such as granulation, coating and drying [35, 39–41]. Previous works on cylindrical spout-fluidized beds [36–38], studied the hydrodynamic and spout characteristics in this type of beds without vibration.

The addition of vibration in aerated hoppers and spout-fluidized beds appears as a promising alternative to be considered in the near future because vibration can reduce the gas minimum fluidization velocity and increase the homogeneity of the granular material. However, the introduction of vibration may promote the appearance of different patterns which may cause large heterogeneities in the bed. Thus, a fundamental characterization of the combined effects of vibration and aeration in triangular or conical shaped beds is paramount to understand and further design these systems.

Regarding the different experimental techniques aimed at characterizing the bed and bubble behavior in fluidized beds, Digital Image Analysis (DIA) and Particle Image Velocimetry (PIV) are frequently used. These techniques make use of pseudo two-dimensional (pseudo-2D) beds (i.e. beds of small thickness), which have been shown to be of great help for the understanding of the bed and bubble dynamics in both conventional and vibrated fluidized beds, as they allow optical access to the bed [42–46]. DIA has been previously applied in vibrated fluidized beds [47, 48] whereas PIV has been extensively used in the characterization of the particle movement in conventional fluidized beds [43, 44, 49–51]. However, the use of PIV in vibrated fluidized beds is still very reduced [52].

The present work aims at clarifying the dynamics of granular systems subjected to vibration in a bed of triangular geometry (i.e. pseudo-2D conical bed) and the influence of gas injection through the inclined

walls of the bed on the surface waves and convective patterns observed in the granular material. Different granular patterns are identified as a function of the vibration frequency, vibration strength and the gas superficial velocity though the inclined walls of the bed. The results here presented constitute a necessary first step on a fundamental understanding of the novel combination of vibration and gas injection in beds of triangular or conical geometry. The potential applications of this research are vibration-assisted systems of triangular or conical geometry like spout-fluidized beds and aerated hoppers. Thus, the present work can serve as a basis for the identification of vibration and gas injection conditions that may improve or deteriorate the operation of this kind of systems.

2. Experimental setup

The experiments were conducted in a triangular pseudo-2D bed that is fluidized with air and vibrated in the vertical direction (Figure 1). The dimensions of the bed are 0.206 m span, 0.2 m height (measured from the vertex of the triangle) and 0.01 m thickness, as shown in Figure 1. The bed front and back walls are made of antistatic PMMA in order to allow optical access to the fluidized bed. Air is introduced to the bed through each of the inclined walls, which form an angle of 45° with the horizontal. The air mass flow is regulated by means of a mass flow controller (Analyt-GFC47) and enters a first plenum and then a second plenum through a gas distributor consisting on 50 holes of 1 mm of diameter (see Figure 1). Then, the air enters the bed through the lateral inclined walls, which are perforated with 80 holes of 0.5 mm of diameter (40 holes in each wall). Due to the configuration of the bed air was not injected through the vertex of the triangular bed. However, particles located in the vertex of the bed are not static as they are affected by vibration and the motion of the surrounding particles.

[Figure 1 about here.]

The whole bed was mounted onto an electrodynamic shaker (Labworks Inc., ET-139). A controller (Labworks Inc. VL-144), amplifier (Labworks Inc., PA-138-1) and an accelerometer (PCB Piezotronics Inc., J352C33) were used to generate and control a sinusoidal vibration $\delta = A\sin(2\pi ft)$, where δ is the bed displacement, A is the vibration amplitude and f is the vibration frequency. Due to the characteristics of the experimental facility, vibration frequencies larger than $f > 30$ Hz and vibration strengths, $\Gamma = A(2\pi f)^2/g$, larger than $\Gamma > 10$ had to be avoided. The front part of the bed was uniformly illuminated by two LED spotlights symmetrically disposed at each side of the bed.

The bed was filled up to the top of the inclined walls with ballotini glass beads with a mean diameter of $d_p = 1.15$ mm. Approximately a 5% of the particles were black to enhance the correlation during the processing of results with Particle Image Velocimetry (PIV). The minimum fluidization velocity of the particles under static conditions was measured by means of the change of slope of the mean pressure drop

of a pressure sensor located in the first plenum and resulted to be $U_{mf} = 0.41$ m/s. A high speed camera (Optronics CL 600 x2/M) was used to record images through the front wall of the bed at a frame rate of 200 images per second during 20 seconds.

It has been reported that a particle diameter/transverse thickness ratio of ∼0.1 has been shown to be sufficient to ensure a freely fluidized system, despite the fact the walls introduce frictional effects that may affect the solids velocity [53]. The effect of the walls on the particles is twofold. On the one hand, the walls tend to decrease the solids velocity due to friction. On the other hand, the walls introduce vibration energy to the system which assists the fluidization of the particles.

The effect of vertical vibration on the dynamics of the vibrated triangular fluidized bed was studied in a twofold way. Firstly, a qualitative observation of the granular patterns of the bed was carried out. The different transitions in the flow regimes for a variety of vibration strengths, Γ, were qualitatively identified as a function of the vibration frequency, f and for different gas superficial velocities under, equal and above the minimum fluidization velocity, including the case of no gas injection (i.e. U_0/U_{mf} =0, 0.7, 1 and 1.2). Secondly, once the flow regimes were identified, PIV measurements were undertaken in order to study the motion of particles in the triangular bed for the experimental conditions depicted in Table 1.

[Table 1 about here.]

3. Data processing

The particle velocity between two consecutively recorded images was obtained by means of PIV using the multigrid code MATPIV [54]. The PIV measures the instantaneous velocity of solids by dividing the domain in smaller sections (i.e. interrogation windows) and by cross-correlating these sections; the most probable displacement of the particles in each window is calculated. A mask is applied to the original image so that the velocity vectors are only calculated in the interrogation windows pertaining to the bed bulk [54]. In the present work, interrogation windows of 32x32 pixels and 50% overlap were employed for the calculation of the velocity of particles in the bed. Six reference squares were glued to the front wall of the bed vessel in order to follow its instantaneous displacement. To improve the accuracy and stability of the velocimetry technique, this displacement was subtracted in the particle images before performing the PIV calculations, so that, instead of using an absolute reference system in which the bed is oscillating, the PIV algorithm calculates the displacement of particles in a relative reference system that moves with the bed vessel. The relative average velocity of particles along an experiment was calculated as:

$$\overline{U}_s = \sum_{i=1}^{N} U_i(x, y)/N \tag{1}$$

where $U_i(x, y)$ is the instantaneous velocity of particles in the i^{th} frame at a location (x, y) and N is the number of frames in an experiment.

It was observed in the experiments that the oscillation of the bed bulk presented a cyclic behavior with an overall period of oscillation (i.e. time required to repeat a complete oscillatory movement) of the bed bulk that may vary depending on the experimental conditions. This period was found to be, $T_o = n_p/f$ with $n_p = 1, 2$ and 4 being the number of bed vessel cycles completed in a period of oscillation of the bed bulk. The bed follows a cyclic and sinusoidal behavior, so the results can be also analyzed as a function of the phase of the oscillation cycle. Thus, the velocity vectors pertaining to a given range of phases of the bed vessel vibration (viz. phase intervals) were averaged, obtaining a phase velocity map for each of the phase intervals in which the period of oscillation is divided. In order to study the particle velocity as a function of the position of the bed vessel, T_o was divided into $k = 4n_p$ phase intervals of analysis to capture the phase behavior of the particles of the bed with a phase resolution of $\Delta\phi = \pi/2$. The average velocity in every phase interval $\phi_k = [\pi(k-1)/2, \pi k/2]$ can be calculated as:

$$\overline{U}_{s,\phi_k} = \frac{\sum_{i=1}^{N} U_{s,i}(x, y)\delta_{i,k}}{\sum_{i=1}^{N} \delta_{i,k}} \tag{2}$$

where $\delta_{i,k}$ is equal to the unity if the phase ϕ_i in the i^{th} frame is within the phase interval ϕ_k:

$$\delta_{i,k} = \begin{cases} 1 & \text{if } \frac{k-1}{2}\pi < \phi_i < \frac{k}{2}\pi \\ 0 & \text{otherwise} \end{cases} \tag{3}$$

4. Results and discussion

The following sections study the dynamics of the particles in the vibrated fluidized bed. Firstly, the general bed behavior is described and different granular patterns are detected. Then, the convective motion (*viz.* gulf stream circulation) of particles in the bed is characterized using the time−averaged velocity of particles. Finally, to further explain the origin of the gulf stream motion and the occurrence of a reversal in its direction, the cyclic particle motion is analyzed as a function of the phase in a period of vibration.

4.1. General bed behavior

Under conventional fluidization conditions, i.e. the air is introduced through the inclined walls and the bed is not vibrated, there is no particle motion for $U < U_{mf}$ and bubbles appear for $U > U_{mf}$, which rise close to the inclined walls.

It was observed that the combination of vibration of the bed and gas injection through the inclined walls of the bed drastically changed the way particles behave in the bed, promoting the formation of granular patterns in the bed. In the case the bed vessel is not vibrated the particles presented a behavior similar

to that of a conventional fluidized bed. That is, the bed is fixed for gas superficial velocities below U_{mf}, whereas bubbles, which tended to rise close to the lateral walls of the bed, commence to appear for gas superficial velocities above U_{mf}. Figure 2 shows the different granular patterns observed in the triangular bed when the bed is vibrated with different combinations of the vibration frequency, vibration strength and gas superficial velocity. In Figure 2(a), Faraday tilting is the dominant behavior [26]. Here, the bed is lifted by vibration ($\Gamma > 1$) and the particles roll down in the inclined surface of the bed and move up through the bulk of the bed. In Figures 2(b) and 2(c), surface waves with formation frequencies $f/4$ and $f/2$ (i.e. the frequency of the surface waves is one quarter or one half of the excitation frequency, respectively), are observed. These surface waves are similar to those produced in rectangular and circular beds [12, 26]. Figures 2(d-f) schematize the different convective patterns observed in the triangular bed for the range of vibration conditions tested. In Figure 2, vibration conditions and gas fluidization velocities have been selected to exemplify the most characteristic surface waves and convective patterns detected in the experiments.

In Figure 2(d), a convective motion with a downflow of particles at the center of the bed takes place. Interestingly, if the gas injection through the lateral walls is large enough, the gulf-stream motion of particles in the bed could be reversed, as depicted in Figure 2(e) and 2(f). Regardless the particles move upwards and downwards at the center of the bed, the particles at the extreme sides of bed barely mix. This may induce the presence of large heterogeneities in the bed in chemical conversion processes.. Figure 2(f) represents a case in which an inflexion point in the central section of the bed, with upward and downward motion above and below it, respectively, could be observed. A net downward displacement of particles could be observed close to the front and rear walls of the bed and the particles are transported to the top of the bed inside the bulk between these walls. Also, in Figure 2(f), vibration causes the whole bed to cyclically detach from the inclined walls, which probably have and influence in making the side walls convection observed in Figure 2(e) to disappear. In particular, in Figure 2(e) an upward vertical motion of particles is observed in the center of the bed, whereas the convection cells are very small and are situated close to the side walls.

[Figure 2 about here.]

Figure 3 shows the time-averaged solids relative velocity obtained with PIV in the vibrated triangular fluidized bed for different combinations of the vibration amplitude, vibration frequency and gas superficial velocities. In general, for the case with no gas injection through the lateral walls of the bed, the only convective motion observed is similar to the one shown in Figure 3(a) for $f = 15$ Hz and $\Gamma = 3.5$ with a downward displacement of particles in the central part of the bed. and downward close to the inclined walls of the vessel. The result is a convective motion of the bed particles (i.e. gulf stream circulation). Here, the bed bulk is cyclically lifted from the inclined walls with a frequency equal to the frequency of vibration of the bed. The convective motion observed in Figure 3(a), will be denominated hereafter as "downward convection".

When increasing the gas superficial velocity while keeping the same Γ and f, different convective patterns were observed. Figure 3(b,c,e,f,g) represents the velocity vectors for the example case of $f = 15$ Hz, $\Gamma = 3.5$ and gas superficial velocities of $U_0/U_{mf} = 0.7, 0.9, 1, 1.1$ and 1.2, respectively. For a gas superficial velocity of $U_0/U_{mf} = 0.7$ in Figure 3(b), the whole bed bulk separates from the lateral walls of the bed with a period $T_o = 2/f$, i.e. the particles in the bed repeat the same pattern every 2 cycles of the vessel vibration. In Figure 3(b), the downward motion of particles found in Figure 3(a) in the center of the bed is still present. Increasing the gas superficial velocity from $U_0/U_{mf} = 0.7$ (Figure 3(b)) to $U_0/U_{mf} = 0.9$ (Figure 3(c)) does not promote a significant change on particle average velocity in the bed. In these cases of $U < U_{mf}$ it was visually observed that a three dimensional convective motion of particles appears, which is induced by the interaction of the particles with the front and rear walls of the bed. In general, when air is introduced through the distributor of the bed, particles move down close to the front and back walls of the bed and move up through the middle section between these walls. These 3D effects are manifested in Figures 3(b) and 3(c) through an uniform field of descending velocity vectors on the transparent front wall of the bed.

Noticeably, for $f = 15$ Hz and $\Gamma = 3.5$, when the gas superficial velocity is equal or above U_{mf} ($U_0/U_{mf} \geq 1$), (see Figure 3(e-g)), a reversal of the previously described downward convection of the bed particles is observed. Particles ascend now in the central section of the bed and descend in the regions closer to the inclined walls (see Figure 3(e)). For the sake of simplicity, this pattern of upward convection of particles in the central region of the bed will be referred in the present work as "reverse convection" since it has opposite direction to the pattern found in Figure 3(a). Figure 3(h) schematically shows the behavior of particles in the bed when this reverse convection occurs. The region in which the particles ascend is delimited by the presence of two inflexion points (i.e. locations with null average velocity) in the central section of the bed at different heights, which separate the ascending or descending average displacement of particles. Another two inflexion points are symmetrically located at the same height at both sides of the bed. These last inflexion points are centers of the two main convective cells formed in the bed. In Figure 3(e-g), two regions with different convective motions can be clearly distinguished in the triangular bed: the central part of the bed (from around $x = 0.04$ m to $x = 0.16$ in Figure 3(g)) and the two regions close to the side walls. These two regions behave similarly to the arching structures in rectangular granular beds, see [17], in which arches alternatively detach from the bottom of the bed and present an upward convective motion of particles on their central section and downwards in the boundary between the two arches (see Figure 3(h)). The size of the arch formed on the region close to the bed lateral walls, increases with the gas velocity in Figures 3(e-g). Further increase of the gas superficial velocity under the same vibration conditions leads to the formation of bubbles close to the sidewalls of the bed and, again, to a downward convection of particles in the central section of the bed. If the vibration strength Γ is large enough, for $U_0/U_{mf} = 1$ (Figure 3(d)), the size of the zone in which the arching structures appear is very reduced and the bed bulk completely detaches from the inclined bed. The period of oscillation of the bed bulk in this case is $T_o = 3/f$.

[Figure 3 about here.]

In order to characterize the vibration and gas conditions that lead to the different granular patterns encountered in Figures 2 and 3, Figure 4 depicts the transition maps resulting from varying Γ and frequency f for four different gas superficial velocities. For the case of no gas injection, the particles started to appreciable show convective motions for ($\Gamma > 1$). For $1.2 < \Gamma < 1.8$ Faraday tilting (see Figure 2(a)) prevails. The convective pattern described in Figure 3(a) was observed in the experiments for values of the vibration strength between 1.8 and 3.75. Further increase of the vibration amplitude to values $\Lambda = 3.5 - 4$ promoted the formation of surface waves of period $T_o = 4/f$ (see Figure 2(b)). As mentioned above, the dependence of the particle behavior on the vibration frequency and amplitude changed dramatically when gas was injected through the inclined walls. This may be attributed to an increase of the bed voidage with increasing gas flow, affecting critically the interaction between particles and the walls and, in turn, the propagation of the vibration inside the bed bulk. The effect of U_0/U_{mf} on the particles flow pattern can be seen in Figure 4(b-d) which shows the transition maps for gas superficial velocities under, equal to, and above the minimum fluidization velocity. For a gas superficial velocity of $U_0/U_{mf} = 0.7$, an intricate transition map was obtained, in which surface waves of frequency $f/2$, $f/4$ and reversed convection were obtained for narrow ranges of Γ (i.e. operative windows). For the same vibration frequency, up to seven different motions could be observed when progressively increasing Γ: no motion of particles, motion of particles in an unordered fashion, $f/2$ surface waves, jump mode in which the bed bulk fully detached from the inclined walls, $f/4$ surface waves and an unstable mode in which particles did not find a stable granular pattern. In general, the value of Γ required to a specific bulk motion to appear decreases with f. The operative window for reverse convection observed in Figure 4(b) broadened when increasing the gas superficial velocity to $U_0/U_{mf} = 1$ in Figure 4(c). In this case, four different particle behaviors were encountered when increasing Γ. For low vibration amplitudes, the particles appreciably moved in the bed without following an ordered pattern. Increasing the vibration amplitude promoted the formation of the so called reversed convection. An unstable mode, serving as a transition between the reversed convection and jump modes depicted, respectively, in Figures 3(e) and 3(f) was observed when further increasing Γ. Finally, when increasing the gas superficial velocity beyond U_{mf}, as shown in Figure 4(d), only two modes were observed. In this case, for a fixed f, if the vibration strength was small enough, a convective motion with particles moving downwards in the center of the bed was observed. However, when increasing the vibration amplitude, there was a value of Γ beyond which the reversed convection of particles was found, with a behavior similar to that described in Figure 2(e). The vibrational strength at which the convective motion is reversed increases with f. This implies that for a sufficiently high superficial gas velocity, the reversal of the gulf stream is suppressed by increasing the vibration frequency.

[Figure 4 about here.]

4.2. Particle gulf stream motion in the bed

Figure 5 shows the effect of the vibration strength on the reversed convection pattern of the time-averaged particle velocity described in Section 4.1. The gas superficial velocity of the experiments was $U_0/U_{mf} = 1.2$ and the vibration conditions were $f = 15$ Hz and $\Gamma = 1.5 - 3.5$. According to Figure 4(d), these operative conditions ensure the presence of cases in which downward convection ($\Gamma = 1.5$ and 2) and reversed convection ($\Gamma = 2.5, 3$ and 3.5) are observed.

Figures 5(a,b) confirm the regimes defined in Figure 4(d), i.e. for $\Gamma \lesssim 2.4$. A downward convection pattern is observed with particles moving downwards in the central section of the bed and upwards close to the inclined walls. Two recirculation vortexes are formed close to the inclined walls of the bed due to the change from ascending to descending motion of the particles in that region of the bed.

An increase of the vibration strength to values $\Gamma \gtrsim 2.4$ promotes the reversion of the gulf stream motion of the bed. For $\Gamma = 2.5$ (Figure 5(c)), the area with upward velocities of particles (viz. reversed gulf stream motion) is smaller than for $\Gamma = 3$ and $\Gamma = 3.5$ in Figure 5(d,e), due to its closeness to the transition between the downward convection and the reverse convection. Also, for this vibration strength, the period of the bed bulk oscillation is $T_o = 2/f$, i.e. the bed bulk repeats the same granular motion every two oscillations of the bed vessel. An increase of Γ within the range of operation tested does not seem to promote significant changes in the position of the arching structures formed close to the lateral walls of the bed. However, the period of oscillation of the bed bulk motion in the cases of $\Gamma = 3$ and 3.5 is $T_o = 4/f$, which implies that the bed bulk repeats the same oscillatory behavior every four vibration cycles of the bed vessel. Besides, the average velocity of particles in the boundary between two arches ($x = 0.04$ m and $x = 0.16$ m in Figure 5(c-e)) increases when increasing the vibration strength due to the more vigorous oscillation of the bed bulk. This manifests that the velocity of the convective rolls formed in the bed is sensitive to the vibration amplitude. However, the velocity of the reversed gulf stream circulation in the central region of the bed does not greatly change when increasing Γ.

[Figure 5 about here.]

Figure 6 shows the average velocity vectors superimposed to the average velocity magnitude for experiments conducted for the same gas superficial velocity ($U_0/U_{mf} = 1.2$) and vibration strength ($\Gamma = 3.5$) and different vibration frequencies f =14, 15 and 16 Hz. In Figure 6, the average velocity of the particles in the bed slightly decreases as the frequency of vibration of the bed vessel increases. This can be clearly appreciated in the velocity magnitude between the arching regions formed in the bed. Note that the vibration amplitude decreases when increasing the vibration frequency for the same Γ (4.4 mm for 14 Hz, 3.8 mm for 15 Hz and 3.4 mm for 16 Hz). The results depicted in Figure 6 reveal that the downward velocity of particles between the arching regions is slightly higher for the cases with bigger vibration amplitudes. Thus, it can be deduced that the velocity of the particles is mainly affected by the vibration amplitude and

not by the vibration strength (see also Figure 5). However, as in Figure 5, the upward velocity of particles in the central section of the bed is not strongly affected by the change in the vibration frequency. Besides, from a qualitative point of view, a slight change of position and a loss of symmetry of the four inflexion points in the bed that can be observed in Figure 6 for the cases of $f = 14$ Hz and $f = 16$ Hz. This can be explained taking into account that the reversal of the gulf stream motion and the appearance of inflexion points in the bed (Figure 3(h)) is induced by vibration that is transmitted to the bed by the collision of the bed bulk with the inclined walls. If the bed bulk detaches (at least partially) from the bed in a non perfectly symmetrical way, particles would impact one of the inclined walls earlier than the other, and this promotes the asymmetry of the inflexion points.

[Figure 6 about here.]

4.3. Particle motion as a function of the vibrating phase

It has been seen in the previous sections that mean values of particle velocity define recirculations that can be reversed for certain conditions. Also, when the reversed motion occurs, inflexion points appear. In order to study the origin of the reversed recirculations and inflexion points, this section analyzes the behavior of the particle velocity in the triangular bed as a function of the phase in the vibration period (see Section 3). The results are analyzed as a function of the phase of the oscillation cycle. This type of analysis helps to understand the average motion of solids in the bed, for example the downward convective motion or the propagation of the wave of solids velocity.

Figure 7 presents the results of the phase averaged velocity vectors (Equation (2)) for the case of $f = 15$ Hz, $\Gamma = 3.5$ and no gas injection through the bed inclined walls. This combination of f and Γ has been selected to ensure the presence of recirculation patterns of particles for the case of no gas injection through the inclined walls of the bed and for the case of $U_0/U_{mf} = 1.2$ shown in Figure 8 (see Figure 3(a,g)). Here, ϕ_v represents the phase of the bed vessel displacement, with $\phi_v = 0 - 0.5\pi$ corresponding to the bed vessel moving upwards from the central to the highest vertical position. In the interval $\phi_v = 0.5\pi - 1.5\pi$ the bed bulk detaches from the inclined walls due to the inertia of the particles, i.e. the bed vessel starts to move downwards but the bed bulk keeps on moving upwards because $\Gamma > 1$. Due to this, the average particle motion in Figure 7 in the intervals $\phi_v = 0.5\pi - \pi$ and $\phi_v = \pi - 1.5\pi$ presents a net upward displacement (relative to the bed vessel). Note that the slightly higher velocity magnitude of particles in the top part of the bed, close to the freeboard of the bed, for the interval $\phi_v = \pi - 1.5\pi$ reflects the expansion of the bed bulk. The particles in the top part of the bed, as they support a smaller mass of particles above them, move more freely than the particles in the lower layers and present a larger upward velocity. The contact between the bed inclined walls and the bed bulk takes place in the phase interval $\phi_v = 1.5\pi - 2\pi$ when the ascending bed vessel impacts the descending bulk of the bed. This can be deduced in Figure 7(a) as a result

of the decrease of the average particle velocity in a reduced region close to the walls in that phase interval. In order to further describe the effect of the impact of the bed vessel on the bulk motion, Figure 7(b) details the averaged velocity vectors presented in Figure 7(a) for a phase interval $\phi_v = 1.75\pi$ to $\phi_v = 0.06\pi$ of the next cycle. In that phase interval, the bed impacts the inclined walls of the bed at around $\phi_v = 1.75\pi$. From that phase moment on, the velocity maps of the bed present in Figure 7(b), two distinguishable regions in the intervals $\phi_v = 1.94\pi - 2\pi$ and $\phi_v = 0 - 0.06\pi$: one central region (α in Figure 7(b)) that maintains the downward velocity of the particles relative to the walls due to gravity, and a progressively growing region in which particles are slowed down by the collision of particles with the inclined walls (β, η), similar to that encountered in [28]. In Figure 7(b), the red and blue lines delimit the solids velocity magnitude U_s = 0.2 m/s and U_s = 0.5 m/s, respectively. These two velocities have been selected as they can define the progression of the solids velocity wave inside the bed. The displacement of these curves to the central region of the bed reveals the presence of a mechanism of wave propagation inside the bed caused by the impact of the bed bulk with the the inclined walls [45]. The velocity of propagation of this velocity perturbation can be calculated as the distance employed by the U_s = 0.2 m/s and U_s = 0.5 m/s velocity contours presented in Figure 7(b) to cover the propagation distance parallel to the inclined bed walls divided by the time needed to cover that distance. The mean propagation velocities calculated for the red and blue contours between $\phi_v = 1.75\pi$ and 0.06π in Figure 7(b) are $V_{prop,0.2}$ = 5.8 m/s and $V_{prop,0.5}$ = 5.5 m/s, respectively. The relative displacement of particles in the central section of the bed (α) with regard to the displacement in the regions close to the inclined walls (β, η) shown in Figure 7(b), promotes the formation of the convection cells observed in Figure 3 when no gas is injected through the lateral walls of the bed.

[Figure 7 about here.]

Figure 8 shows the solids phase averaged velocity in the bed for the case of f = 15 Hz, Γ = 3.5 and a gas superficial velocity of $U_0/U_{mf} = 1.2$. In addition to the reversal motion of particles in the bed, it was observed in the recorded images that the main frequency of oscillation of the bed bulk was equal to the vibration frequency of the bed vessel, f. However, injection of gas through the bed inclined walls made these oscillations of the bed bulk not totally similar to each other and the bed required four consecutive vibration cycles of the vessel to repeat the same granular pattern. Therefore, gas injection at $U_0/U_{mf} = 1.2$ through the bed inclined walls increased the overall period of oscillation of the bed bulk to $T_o = 4/f$. In consequence, an overall cycle of the bed bulk oscillation were composed of four consecutive subcycles (subcycles 1 to 4 in Figure 8). Each subcycle covers a time period equal to the vibration period of the bed vessel, T. In Figure 8, each row (e.g. Figures 8(a) to 8(b)) comprises a subcycle. The first column of Figure 8 contains the velocity vectors in the triangular bed time averaged over a subcycle. Thus, the average of the velocity vectors in the first column of Figure 8 corresponds to the overall time averaged particle velocity, which is shown in Figure 3(g). The next columns of Figure 8 represents the phase averaged particle velocity (see

Section 3) resulting from averaging the velocity vectors over a vibration phase intervals of size $\Delta\phi = \pi/2$.

In Figure 8 there are two clearly distinguishable regions in the bed, i.e. the central section of the bed, close to x =0.1 m, and the lateral region, close to the bed lateral corners. These two regions present opposite vertical particle average velocities in each of the subcycles studied in the figure. When the particles in the central section of the bed have an average ascending velocity, the ones belonging to the region close to the lateral corners present a descending velocity and vice versa. The bed bulk impacts the bed vessel close to the vertex of the triangle just before the first subcycle (Figure 8(a)) and a compression wave of particles propagates upwards inside the central region of the bed between Figure 8(d5 and a2), which decreases the velocity of the particles in that region. Once the bed vessel commences its descending motion ($\phi = \pi/2$ in Figure 8(a3)), the particles in the bed bulk ascend (relatively to the bed vessel) due to their inertia. However, the phase averaged velocity of particles in the phase interval $\phi = \pi/2 - \pi$ in each of the subcycles (Figures 8(a3,b3,c3 and d3)) are different from each other because in the previous phase interval the collision points of the particles with the inclined walls occurred at different locations. This causes the particles in the central and lateral regions of the bed to move with a different relative velocity. In the next phase interval, $\phi = \pi - 3\pi/2$, the difference in the relative velocity of the central and lateral regions is more noticeable. Finally, during the phase $\phi = 3\pi/2 - 2\pi$, the bed bulk presents a net relative downward motion as the bed vessel is moving upwards.

In the second subcycle of oscillation of the bed (Figure 8(b)), the impact of the particles with the vessel takes place in a region of the inclined walls close to the bed lateral walls. Thus, the interval $\phi = 0 - \pi/2$ (Figure 8(b2)) presents a descending motion of particles in the central region of the bed while particles are still unaffected by the presence of the inclined walls. Besides, the particle motion in the lateral region is impeded due to the presence of the inclined walls. In the next two fractions of the cycle, $\phi = \pi/2 - 3\pi/2$, Figures 8(b3, b4), the region close to the lateral walls present a larger upward velocity and the particles in the central region of the bed are compacted. This eventually promotes the earlier impact of the central region of the bed bulk with the inclined walls of the bed in a region close to the bed vessel vertex. However, differently to the first subcycle (Figure 8(a)), when the impact of particles with the bed vessel takes place between the second and the third subcycle (Figure 8(b,c)), the central region of the bed impacts the bed inclined walls over a wider surface, which promotes a different behavior of the particles in the bed along the third and fourth subcyles of vibration (Figure 8(c,d)). All the phenomena previously described and the differences in the relative velocity of particles in the two distinguishable regions in the bed promote the formation of the time-averaged recirculation patterns shown in Section 4.2. This indicates that the four inflexion points found when averaging the velocity vectors along an experiment are points of average velocity equal to zero caused by the composition of opposed relative velocities resulting from each subcycle of bed bulk oscillation.

If the amplitude of the bed vessel vibration is sufficiently small, for example f = 15 Hz, $U_0/U_{mf} = 1.2$

and $\Gamma = 2.5$ in Figure 5(c), the period of oscillation of the bed vessel was found to be $T_o = 2/f$. In this case, only two subcycles of the bed bulk oscillation appear and the reversal of the gulf stream motion is promoted by a particle behavior similar to that observed in the first two subcycles of Figure 8 (a,b).

[Figure 8 about here.]

5. Conclusions

The present work experimentally studied the effect of the vibration frequency, vibration strength and gas superficial velocity in a triangular fluidized bed that is vertically vibrated. In this novel configuration, the gas was injected through the inclined walls of the bed. When no gas was injected, different granular patterns could be observed. These patterns were similar to those reported for rectangular and circular beds, e.g. Faraday tilting, $f/4$ surface waves and a gulf stream circulation (i.e. convective motion of particles) due to particles descending through the central section of the bed and ascending close to the inclined walls. However, gas injection through the inclined walls of the bed changed the way particles behave in the bed. Under some vibration conditions, specially if the gas superficial velocity is above, but close, to the minimum fluidization velocity, the gulf stream circulation of particles in the triangular bed could be reversed, leading to particles ascending through the central section of the bed and descending next to the inclined walls. Also, arching structures, which alternatively detach from the inclined distributor of the triangular bed, were formed in a similar way to the arching structures reported for vibrated rectangular beds.

PIV measurements of the particle motion in the bed were employed to identify the cause of the gulf stream reversal and the effects of the vibration frequency and vibration strength on the particle motion in the bed. The results revealed that an increase of the vibration amplitude promotes a higher average velocity of particles close to the inclined walls of the bed. However, the vertical ascending velocity of particles in the central section of the bed was not strongly affected by the vibration amplitude or frequency. Lastly, the PIV results were decomposed into different phase intervals of oscillation in order to understand the behavior of the particles of the bed during a complete oscillation cycle of the bed bulk. For the case of no gas injection through the inclined walls of the bed, the downstream motion of particles through the central section of the bed is produced by differences in the extent of the perturbation on the particle velocity caused by the impact with the inclined walls of the bed. A more intricate phase behavior of particles was observed when gas was injected through the lateral walls. In this situation, several subcycles of vibration appeared depending on the vibration conditions. Particles alternatively ascended and descended in two regions in the bed bulk, similarly to the arching structures in vibrated rectangular beds. The average particle motion after a whole cycle of the bed bulk leads to a net upward motion of particles in the center of the bed and the presence of four inflexion points in the mean particle motion.

The results here presented can serve as a basis for the understanding of granular dynamics in triangular or conical-shaped vibrated beds when gas is injected through the lateral walls. This kind of geometry is used in aerated hoppers and spout-fluidized beds. Thus, these results provide a fundamental knowledge on the effect of the introduction of vibration energy in beds presenting this geometry, which, in turn, may have a deep impact on their performance.

Nomenclature

A = vibration semiamplitude (mm)
d_p = particle diameter (mm)
f = vibration frequency (Hz)
g = gravity acceleration constant (m/s^2)
K = bed thickness (m)
n_p = number of bed vessel cycles (-)
N = number of frames in an experiment (-)
t = time (s)
T = period of vibration (s)
T_o = period of oscillation of the bed bulk (s)
U_0 = gas superficial velocity (m/s)
U_{mf} = minimum fluidization velocity (m/s)
U_s = solids velocity (m/s)
W = bed width (m)
x = horizontal coordinate (m)
y = vertical coordinate (m)

Greek letters
Γ = vibration strength (-)
δ = vibration displacement (m)
ϕ_v = bed vessel vibration phase (rad)

Acknowledgments

This work has been partially funded by the Universidad Carlos III de Madrid (Ayudas a la movilidad 2015) and by the Spanish Ministry of Economy and Competiveness (project ENE2015/00188/001).

References

[1] R. Gupta, A.S. Mujumdar, Aerodynamics of a vibrated fluid bed, Can. J. Chem. Eng. 58 (1980) 332-338.

[2] S. Mori, A. Yamamoto, S. Iwata, T. Haruta, I. Yamada, E. Mizutani, Vibro-fluidization of group C particles and its industrial applications, AlChE Symp. Series. 86 (1990) 88-94.

[3] K. Klusacek, P. Schenider, Stationary catalytic kinetics via surface concentrations form transitient data, Chem. Eng. Sci. 37(10): 1523-1528, 1982.

[4] A. Santos, J. Santamaria, M. Menendez, Oxidative coupling of methane in a vibrofluidized bed at low fluidizing velocities, Ind. Eng. Chem. Res. 34(5):15811587, 1995.

[5] A. V. Vorontsova, E. N. Savinova, P. G. Smirniotis, Vibrofluidized- and fixed-bed photocatalytic reactors: case of gaseous acetone photooxidation, Chem. Eng. Sci. 55(21): 5089-5098, 2000.

[6] R.J. Nelson, C.L. Flakker, D.S. Muggli, Photocatalytic oxidation of methanol using titania-based fluidized beds, Appl. Catal. B. 69(3-4):189-195, 2007.

[7] M. Latifi, F. Berruti, C. Briens, A novel fluidized and induction heated microreactor for catalyst testing, AIChE J. 60:3107-3122, 2014.

[8] H.M. Jaeger, S.R. Nagel, R.P. Behrimger, Granular solids, liquids, and gases, Rev. Modern Phys. 68, 1259-1273, 1996.

[9] M. Faraday, On a peculiar class of acoustical figures; and on certain forms assumed by groups of particles upon vibrating elastic surfaces. Philos. Trans. R. Soc. Lond. 52, 299340, 1831.

[10] F. Zhang, L. Wang, C. Liu, P. Wu, S. Zhan, Patterns of convective flow in a vertically vibrated granular bed, Phys. Lett. A 378 (18-19), 1303-1308, 2014.

[11] E. Clement, L. Vanel, J. Rajchenbach, J. Duran, Pattern formation in a vibrated granular layer, Phys. Rev. E. 53, 29722976, 1996.

[12] H.K. Pak, R.P. Behringer, Surface waves in vertically vibrated granular materials, Phys. Rev. Lett. 71, 1832-1835, 1993.

[13] B. Thomas, M.O. Mason, A.M. Squires, Some behaviors of shallow vibrated beds across a wide range in particle size and their implications for powder classification, Powder Technol. 111, 31-39, 2000.

[14] J.A.C. Gallas, H.J. Herrmann, S. Sokolowski, Convection cells in vibrating granular media, Phys. Rev. Lett. 69, 13711374, 1992.

[15] C. Laroche, S. Douady, S. Fauve, Convective flow of granular mass under vertical vibrations, J. Phys. (Paris) 51, 699-706, 1989.

[16] Y. Taguchi, New origin of a convective motion: elastically induced convection in granular materials. Phys. Rev. Lett. 69, 1367-1370, 1992.

[17] K.M. Aoki, T. Akiyama, Y. Maki, T. Watanabe, Convective roll patterns in vertically vibrated beds of granules, Phys. Rev. E 54, 874883, 1996.

[18] K.M. Aoki, T. Akiyama, K. Yamamoto, T. Yoshikawa, Experimental study on the mechanism of convection modes in vibrated granular beds, Europhys. Lett. 40, 159164, 1997.

[19] T. Akiyama, K.M. Aoki, K. Yamamoto, T. Yoshikawa, Experimental study on vibration-induced convection and heaping in granular beds, Granul. Matter 1, 1520, 1998.

[20] J. Miles, D. Henderson, Parametrically forced surface waves, Rev. Fluid Mech. 22, 143, 1990.

[21] F. Melo, P.B. Umbanhower, H.L. Swinney, Hexagons, kinks, and disorder in oscillated granular layers. Phys. Rev. Lett. 75, 3838, 1995.

[22] S.S. Hsiau, M.S. Wu, Arching phenomena in a vibrated granular bed, Adv. Powder Technol. 99, 185193, 1998.

[23] C.R. Wassgren, C.E. Brennen, M.L. Hunt, Vertical vibration of a deep bed of granular material in a container, J. Appl. Mech. 63, 712719, 1996.

[24] O. Sano, Dilatancy, buckling, and undulations on a vertically vibrating granular layer, Phys. Rev. E. 72, 051302, 2005.

[25] S. Douady, S. Fauve, C. Laroche, Subharmonic instabilities and defect in a granular layer under vertical vibrations. Europhys. Lett. 8, 621627, 1989.

[26] G. Lu, J.R. Third, M.H. Khl, C.R. Mller, On the occurrence of polygon-shaped patterns in vibrated cylindrical granular beds, Eur. Phys. J. E 35, 90, 2012.

[27] J.B. Knight, H.M. Jaeger and S.R. Nagel, Vibration-induced size separation in granular media: the convection connection, Phys. Rev. Lett. 70:24, 3728-3731, 1993.

[28] C.R. Wassgren, M.L. Hunt, P.J. Freese, J.Palarma, C.E. Brennen, Effects of vertical vibration on hopper flows of granular material, Phys. Fluids 14, 10, 2002.

[29] H. Lu, X. Guo, X. Gong, X. Cong, K. Liu, H. Qi, Experimental study on aerated discharge of the pulverized coal Chem. Eng. Sci. 71, 438-448, 2012.

[30] H. Lu, X. Guo, X. Gong, X. Cong, W. Dong, W. Huang Effect of gas type on the fluidization and discharge characteristics of the pulverized coal, Powder Technol. 217, 347-355, 2012.

[31] H. Lu, X. Guo, X. Gong, D. Barletta, M. Poletto, Prediction of solid discharge rates of pulverized coal from an aerated hopper, Powder Technol. 286, 645-653, 2015.

[32] C.E.D. Ouwerkerk, H.J. Molenaar, M.J.W. Frank, Aerated bunker discharge of fine dilating powders, Powder Technol. 72, 241-253, 1992.

[33] C.S. Papazoglou, D.L. Pyle, Air-assisted flow from a bed of particles Powder Technol. 4, 9-18, 1970.

[34] P. Chen, Z. Yuan, C.S. Chyang, F.X. Zhuan, Sawdust discharge rate from aerated hoppers, Particuology 9, 306-313, 2011.

[35] V.S. Sutkar, N.G. Deen, J.A.M. Kuipers, Spout fluidized beds: Recend advances in experimental and numerical studies, Chem. Eng. Sci. 86, 124-136, 2013.

[36] W. Zhong, Q. Li, M. Zhang, B. Jin, R. Xiao, Y. Huang, A. Shi, Spout characteristics of a cylindrical spout-fluid bed with elevated pressure, Chem. Eng. J. 139, 42-47, 2008.

[37] W. Zhong, X. Chen, M. Zhang, Hydrodynamic characteristics of spout-fluid bed: Pressure drop and minimum spouting/spout-fluidizing velocity, Chem. Eng. J. 118, 37-46, 2006.

[38] W. Zhong, M. Zhang, B. Jin, Maximum spoutable bed height of spout-fluid bed, Chem. Eng. J. 124, 55-62, 2006.

[39] K. Mathur, P. Gishler, A study of the application of the spouted bed technique to wheat drying, J. Appl. Chem. 5, 624636, 1955.

[40] L. Marmo, Low temperature drying of pomace in spout and spout-fluid beds, J. Food Eng. 79, 11791190, 2007.

[41] M. Zielinska, M. Markowski Drying behavior of carrots dried in a spout-fluidized bed dryer, Drying Technol. 2007, 25, 261270.

[42] A. Busciglio, G. Vella, G. Micale and L. Rizzuti. Analysis of the bubbling behaviour of 2D gas solid fluidized beds: Part I. Digital image analysis technique. Chem. Eng. J. (2008) 398-413 140.

[43] J.A. Laverman, H. Roghair, M. van Sint Annaland and H. Kuipers. Investigation into the hydrodynamics of gas-solid fluidized beds using particle image velocimetry coupled with digital image analysis. Can. J. Chem. Eng. (2008) 523-535 86.

[44] F. Hernández-Jiménez, S. Sánchez-Delgado, A. Gómez-García and A. Acosta-Iborra. Comparison between two-fluid model simulations and particle image analysis & velocimetry (PIV) results for a two-dimensional gas-solid fluidized bed. Chem. Eng. Sci. (2011) 3753-3772 66.

[45] E. Cano-Pleite, F. Hernández-Jiménez, M. de Vega, A. Acosta-Iborra, Experimental study on the motion of isolated bubbles in a vertically vibrated fluidized bed, Chem. Eng. J., 255 (2014) 114-125.

[46] E. Cano-Pleite, Y. Shimizu, A. Acosta-Iborra and Y. Mawatari. Effect of vertical vibration and particle size on the solids hold-up and mean bubble behavior in a pseudo-2D fluidized bed. Chem. Eng. J. (2016) 384-398 304.

[47] T. Zhou, H. Kage, S. Funaoka, H. Ogura and Y. Matsuno. Fluidization behaviour of glass beads under different vibration

modules. Adv. Powder Technol. (2001) 559-575 12.

[48] Y. Mawatari, K. Tagawa, Y. Tatemoto and K. Noda. Bubbling characteristics under vertical vibration in a two-dimensional fluidized bed. Chem. Eng. Jpn. (2005 18-23 38.

[49] C.R. Müller, J.F. Davidson, J.S. Dennis and A.N. Hayhurst. A study of the motion and eruption of a bubble at the surface of a two-dimensional fluidized bed using particle image velocimetry (PIV). Ind. Eng. Chem. Res. (2007) 1642-1652 46.

[50] D. Santana, S. Nauri, A. Acosta, N. Garcia, and A. Macias-Machín. Initial particle velocity spatial distribution from 2-D erupting bubbles in fluidized bed. Powder Technol. (2005) 1-8 150.

[51] S. Sánchez-Delgado, C. Marugán-Cruz, A. Acosta-Iborra and D. Santana. Dense-phase velocity fluctuation in a 2-D fluidized bed Powder Technol. (2010) 37-45 200.

[52] C. Zeilstra, M.A. van der Hoef J.A.M. and Kuipers. Experimental and numerical study of solids circulation in gas-vibro fluidized beds. Powder Technol. (2013) 153-160 248.

[53] F. Hernández-Jiménez, J. Sánchez-Prieto, A. Soria-Verdugo and A. Acosta-Iborra. Experimental quantification of the particle-wall frictional forces in pseudo-2D gas fluidised beds. Chem. Eng. Sci. (2013) 257-267 102.

[54] J.K. Sveen, MATPIV, 1998-2014, https://www.mn.uio.no/math/english/people/aca/jks/matpiv/.

List of Figures

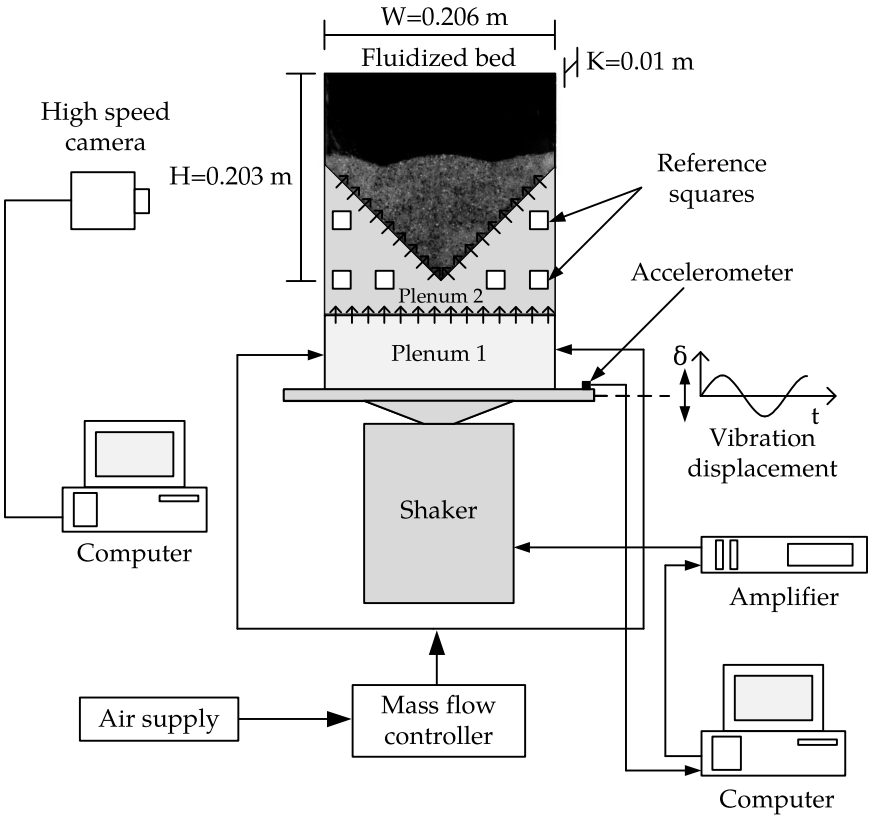

Figure 1: Experimental setup.

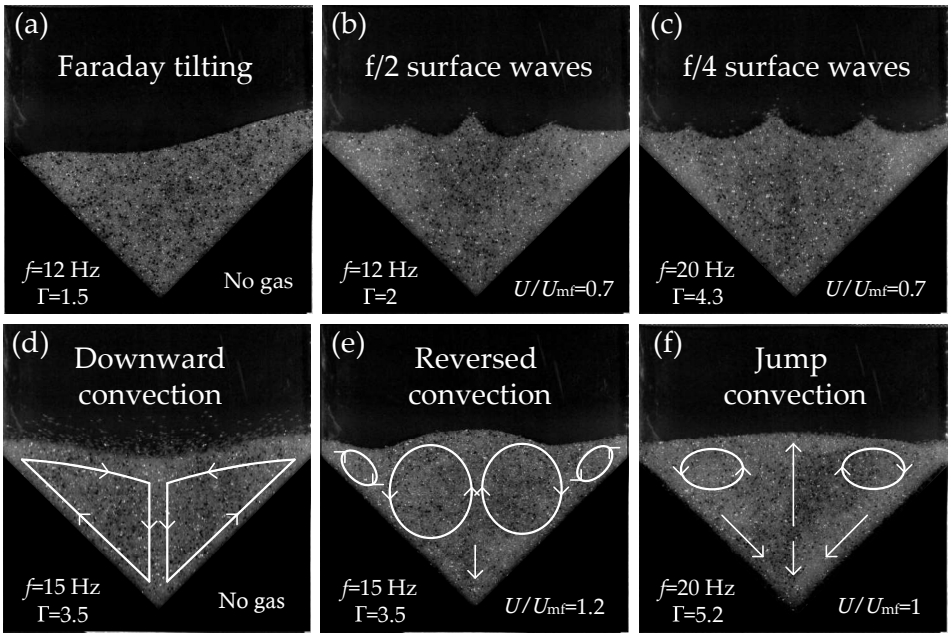

Figure 2: Snapshots of the granular patterns observed in the triangular fluidized bed. (a) Faraday tilting ($f = 12$ Hz, $\Gamma = 1.5$, No gas), (b) $f/4$ surface waves ($f = 20$ Hz, $\Gamma = 4.3$, $U_0/U_{mf} = 0.7$), (c) $f/2$ surface waves ($f = 12$ Hz, $\Gamma = 2$, $U_0/U_{mf} = 0.7$), (d) normal convective motion ($f = 15$ Hz, $\Gamma = 3.5$, No gas), (e) reversed convective motion ($f = 15$ Hz, $\Gamma = 3.5$, $U_0/U_{mf} = 1.2$), (f) jump convective motion ($f = 20$ Hz, $\Gamma = 5.2$, $U_0/U_{mf} = 1$).

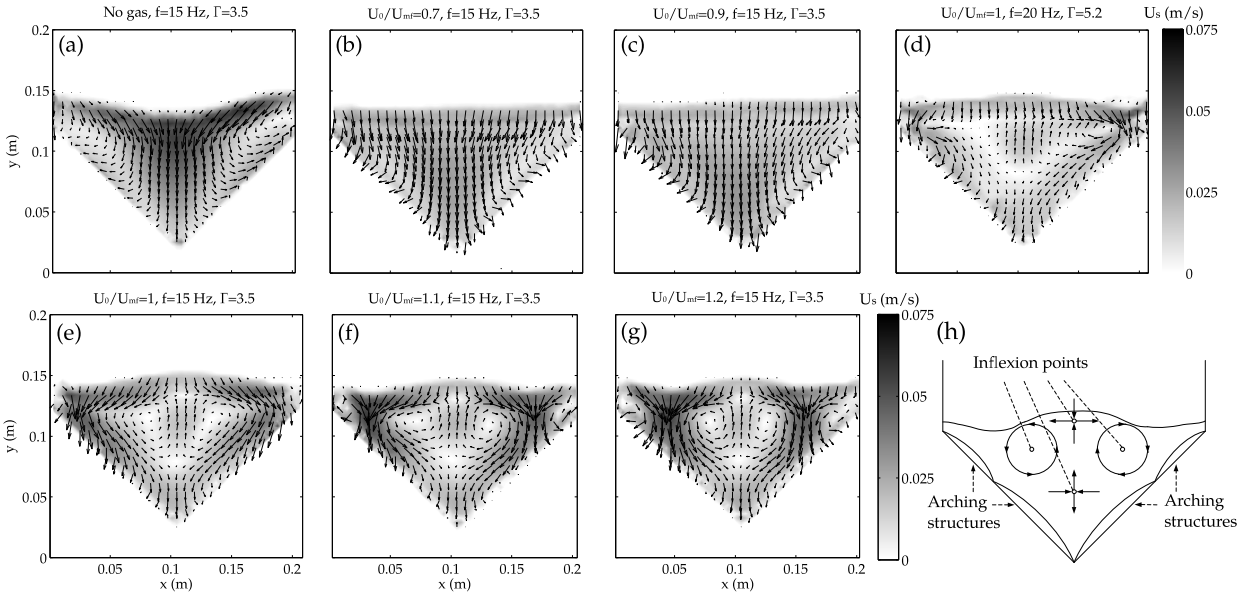

Figure 3: Time-averaged particle velocity in the triangular vibrated fluidized bed for (a) No gas injection, (b) $U_0 = 0.7\ U_{mf}$, (c) $U_0 = 0.9U_{mf}$, (d) $U_0/U_{mf} = 1$, (e) $U_0/U_{mf} = 1$, (f) $U_0 = 1.1U_{mf}$ (g) $U_0 = 1.2U_{mf}$. Results correspond to $f = 15$ Hz and $\Gamma = 3.5$ (a-c, e-g) and $f = 20$ Hz and $\Gamma = 5.2$ (d). The velocity vectors are shown superimposed to the particle velocity magnitude. (h) Schematic behavior of particles in the reversed convection mode.

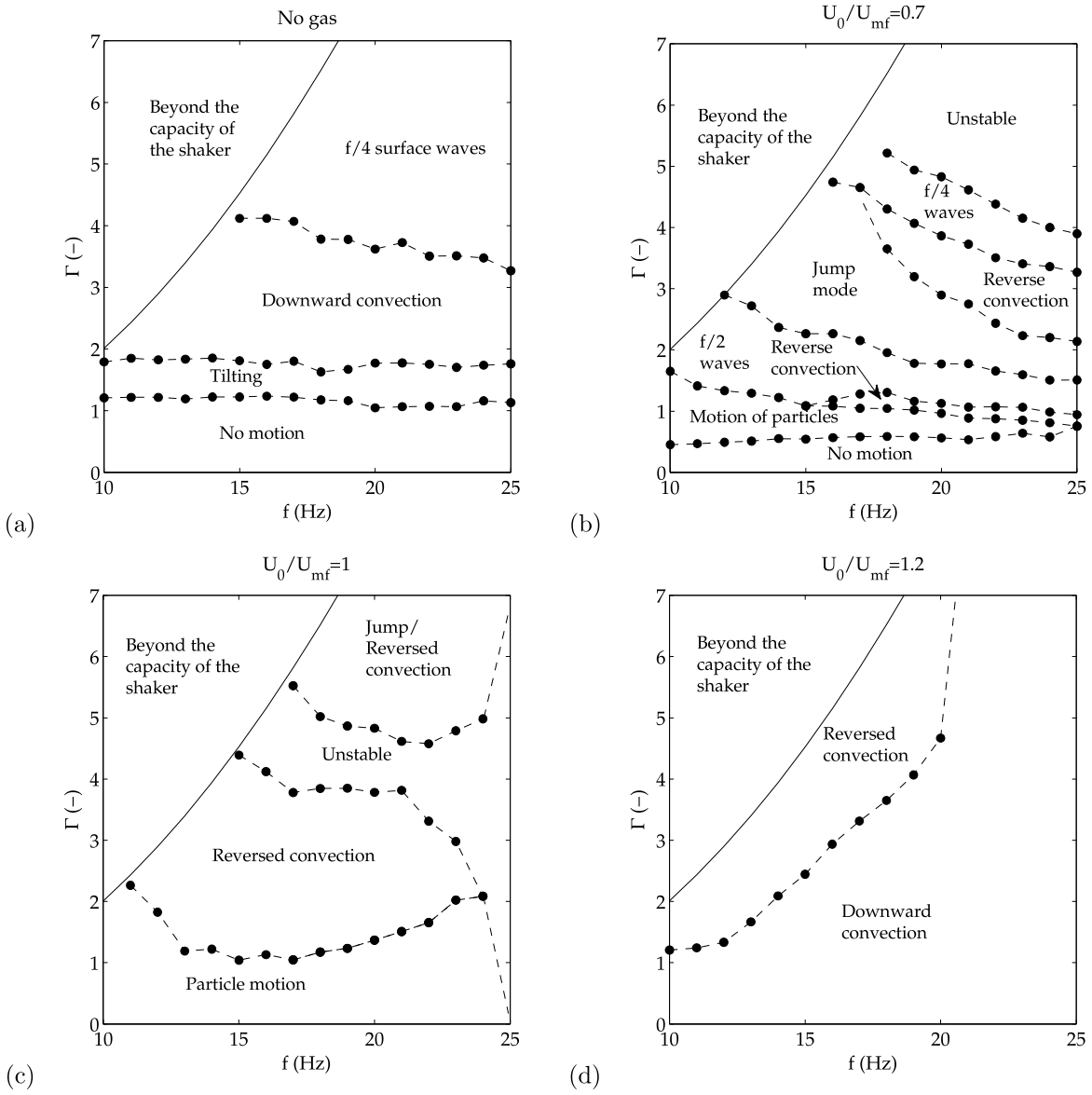

Figure 4: Phase map of the different regimes observed in the vibrated fluidized triangular bed at different gas superficial velocities: (a) No gas injection, (b) $U_0 = 0.7\ U_{mf}$, (c) $U_0 = U_{mf}$ and (d) $U_0 = 1.2\ U_{mf}$.

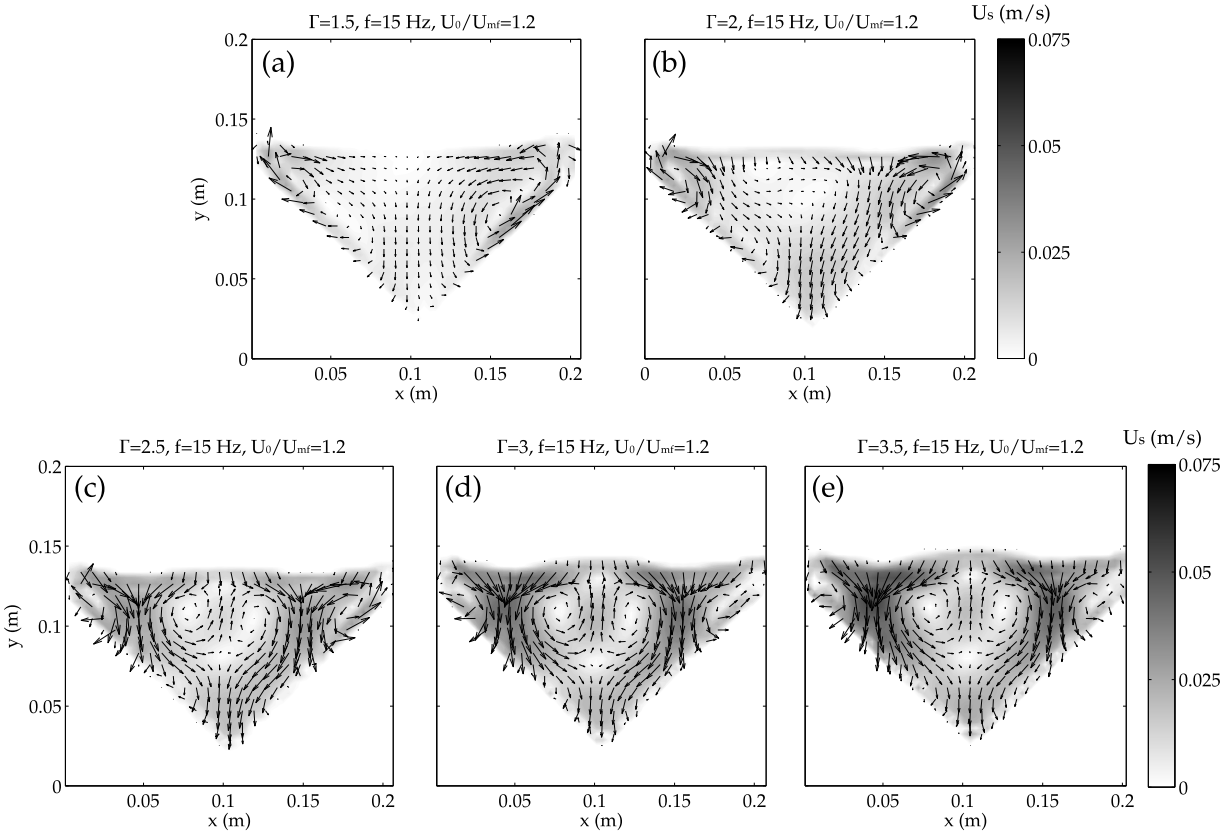

Figure 5: Effect of the vibration strength on the time-averaged particle velocity in the triangular vibrated fluidized bed for $f = 15$ Hz and $U_0 = 1.2\ U_{mf}$: (a) $\Gamma = 1.5$, (b) $\Gamma = 2$, (c) $\Gamma = 2.5$, (d) $\Gamma = 3$ and (e) $\Gamma = 3.5$. The velocity vectors are shown superimposed to the particle velocity magnitude.

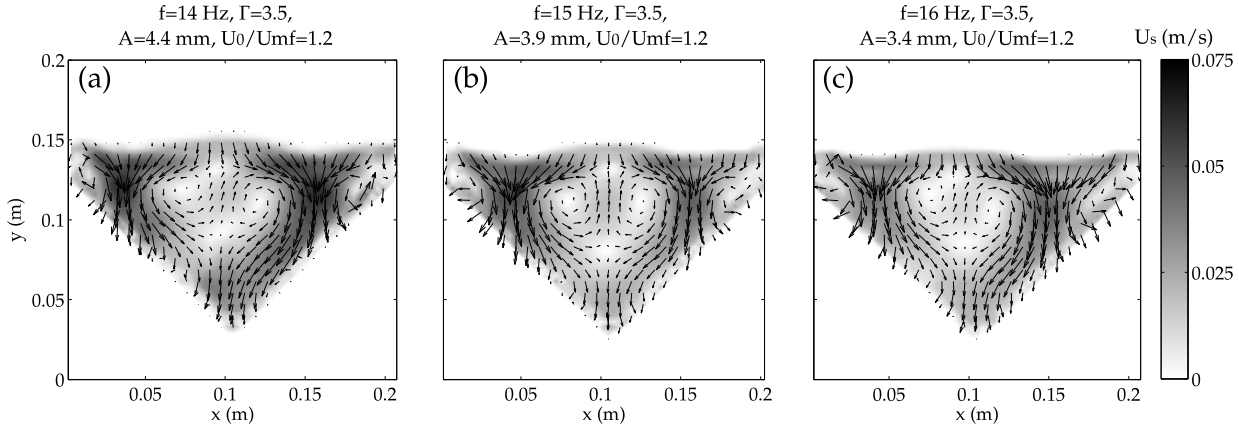

Figure 6: Effect of the vibration frequency on the time-averaged particle velocity in the triangular vibrated fluidized bed for $U_0 = 1.2\ U_{mf}$ and $\Gamma = 3.5$ (a) $f = 14$ Hz, (b) $f = 15$ Hz, (c) $f = 16$ Hz. The velocity vectors are shown superimposed to the particle velocity magnitude.

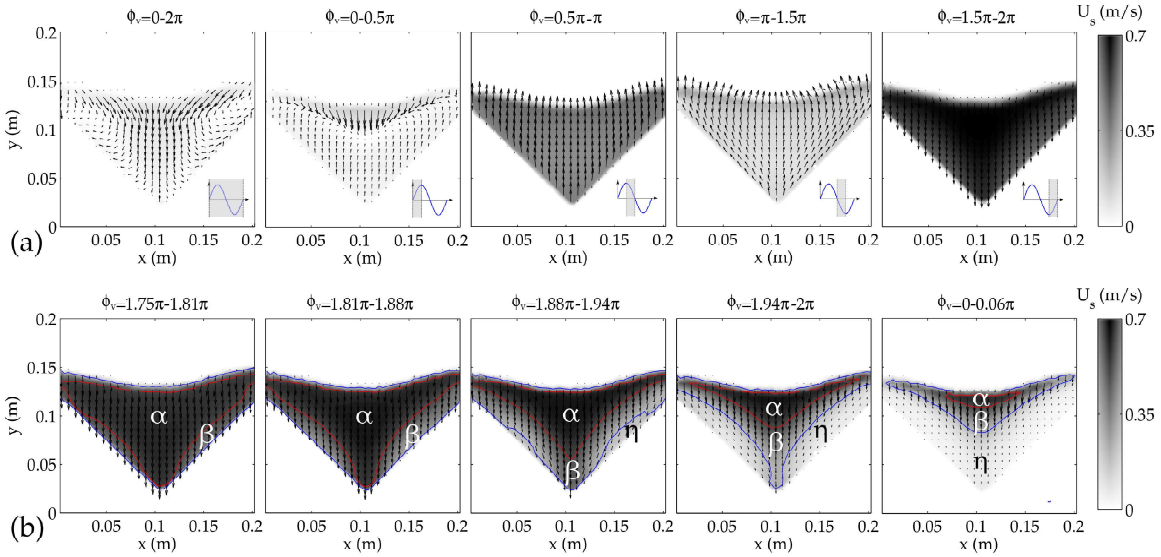

Figure 7: Phase averaged particle velocity in the vertically vibrated triangular bed with $f = 15$ Hz, $\Gamma = 3.5$ and no gas injection. (a) Average oscillation over the complete vibration cycle and for four different phase intervals. (b) Detail of the particle behavior on the interval $\phi = 1.75\pi - 0.06\pi$ (of the next cycle): the blue lines indicate the contours of $U_s = 0.2$ m/s and the red line the contours of $U_s = 0.5$ m/s. The shadowed zone in the cycle represented in the lower right corner of each figure represents the phase interval in which the particle velocity was averaged. The velocity vectors are shown superimposed to the particle velocity magnitude.

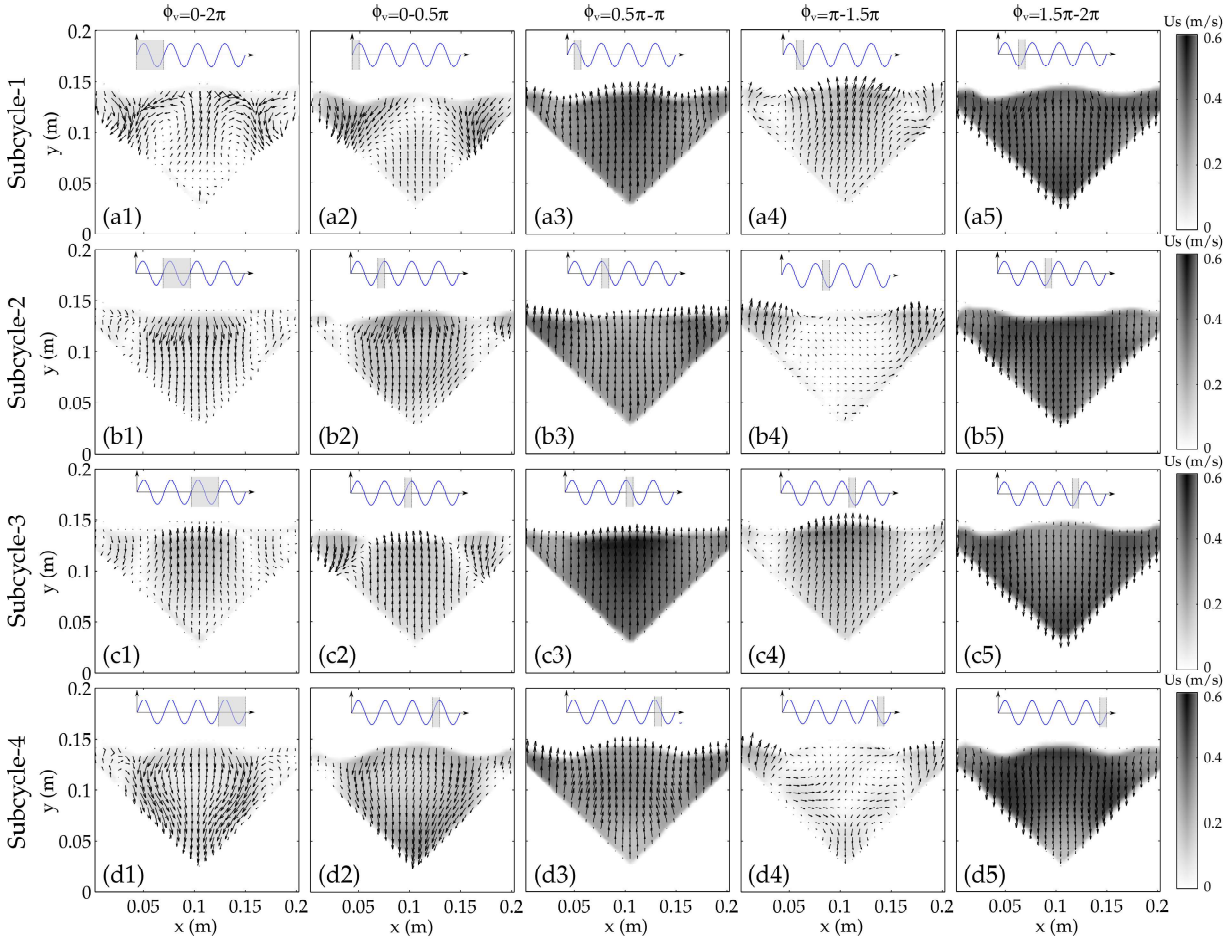

Figure 8: Phase averaged particle velocity in the vertically vibrated triangular bed, $f = 15$ Hz, $\Gamma = 3.5$ and $U_0/U_{mf} = 1.2$ for the four consecutive subcycles of oscillation observed (a-d). The velocity vectors in the first column in the figure represents the particle averaged velocity over a complete subcycle, which corresponds to a vessel vibration cycle $\phi_v = 0 - 2\pi$. The next four columns show the decomposition of the averaged velocities of particles in phase intervals of $\Delta\phi = \pi/2$. The shadowed zone in the vessel displacement included in the lower right corner of each figure represents the phase interval in which the particle velocity was averaged. The velocity vectors are shown superimposed to the particle velocity magnitude.

List of Tables

Table 1: Experimental conditions.

f (Hz)	Γ (-)	A (mm)	U_0/U_{mf} (-)
14	3.5	4.4	1.2
15	1.5	1.7	1.2
15	2	2.2	1.2
15	2.5	2.8	1.2
15	3	3.3	1.2
15	3.5	3.9	0.7, 0.9, 1, 1.1, 1.2
16	3.5	3.4	1.2